Structural Monitoring and Maintenance, *Vol. 3, No. 4 (2016) 377-393*
DOI: http://dx.doi.org/10.12989/smm.2016.3.4.377

Detecting and predicting the crude oil type inside composite pipes using ECS and ANN

Wael A. Altabey*[1,2]

[1]*International Institute for Urban Systems Engineering, Southeast University, Nanjing (210096), China*
[2]*Department of Mechanical Engineering, Faculty of Engineering, Alexandria University, Alexandria (21544), Egypt*

(Received September 24, 2015, Revised November 10, 2016, Accepted November 16, 2016)

Abstract. The present work develops an expert system for detecting and predicting the crude oil types and properties at normal temperature ($\theta = 25℃$), by evaluating the dielectric properties of the fluid transfused inside glass fiber reinforced epoxy (GFRE) composite pipelines, by using electrical capacitance sensor (ECS) technique, then used the data measurements from ECS to predict the types of the other crude oil transfused inside the pipeline, by designing an efficient artificial neural network (ANN) architecture. The variation in the dielectric signatures are employed to design an electrical capacitance sensor (ECS) with high sensitivity to detect such problem. ECS consists of 12 electrodes mounted on the outer surface of the pipe. A finite element (FE) simulation model is developed to measure the capacitance values and node potential distribution of ECS electrodes by ANSYS and MATLAB, which are combined to simulate sensor characteristic. Radial Basis neural network (RBNN), structure is applied, trained and tested to predict the finite element (FE) results of crude oil types transfused inside (GFRE) pipe under room temperature using MATLAB neural network toolbox. The FE results are in excellent agreement with an RBNN results, thus validating the accuracy and reliability of the proposed technique.

Keywords: Electrical capacitance sensor (ECS); Finite Element Method (FEM); crude oil type detection; GFRE composite pipe; Artificial neural network (ANN)

1. Introduction

The petroleum pipelines companies are the companies that to be used for transmission of crude oil with different types and properties from mining countries to customer countries or shipping places. In the most petroleum pipelines companies have one to two pipeline at maximum for transmitting several types of crude oil with different properties at the same time and side by side, because, it is impossible to transmit each type of crude oil in one pipeline alone, this means large pipeline installing area, and high installing cost. Therefore, the economic strategy for these companies aim to transmitting several types of crude oil at the same time in the same pipeline to save the cost. Among the most famous and largest companies in the Middle East, for example,

*Corresponding author, Assistant Professor, E-mail: wael.altabey@gmail.com
[1] Current Affiliation
[2] Previous Affiliation

Copyright © 2016 Techno-Press, Ltd.
http://www.techno-press.org/?journal=smm&subpage=7 ISSN: 2288-6605 (Print), 2288-6613 (Online)

Arab petroleum pipelines company 'SUMED' in Egypt, this large company is for transmitting crude oil coming from Asia countries, especially the gulf countries, where receives the crude oil from the red sea and transmit it with different types in the same pipelines for charging in tanks before shipping in the white sea to customer countries in Europa and America, in order to save time and cost, instead of the other transmission methods. So, one of the major problems in these companies concerns how to separate the crude oil types coming in the same pipelines to charge each type in separate storage tank before shipping to customers.

The common traditional techniques that used in most petroleum pipelines companies are achieved by taking samples from the pipe and analysis them as a function of time, this technique has loss the sensitivity, accuracy and allow to mix the different oil types in the same time, causing financial penalties of companies.

ECS is one of the most mature and promising methods, which measures the capacitance change of multi-electrode sensor due to the change of dielectric permittivity being imaged, and then reconstructs the cross-section images using the measured raw data with a suitable algorithm. It has the characteristics such as low cost, fast response, non-intrusive method, broad application, safety (Yang, Stott *et al.* 1995a, Yang, Beck 1995b, Li and Huang 2000, Mohamad, Rahim *et al.* 2012, Zhang, Wang *et al.* 2014).

ECS was first introduced in the 1980s by a group of researchers from the US Department of Energy Morgantown Energy Technology Center (METC), to measure fluidized bed system (Fasching and Smith 1988, Fasching and Smith 1991, Huang, Plaskowski *et al*. 1989). The technique have been developed rapidly during the past 10 years, and then they have become popular and gained importance to monitor industrial processes due to its low cost and its operability under harsh environmental conditions.

The need for a more accurate measurement of ECS led to the study of the factors which have influence and effect on ECS sensitivity and sensitive domain of ECS electrodes. There are three factors have been studied and found which have effect on ECS measurements, e.g., pipeline material, inner dielectric permittivity (Jaworski and Bolton 2000, Pei and Wang 2009, Al-Tabey 2010, Asencio, Bramer-Escamilla *et al.* 2015, Sardeshpande, Harinarayan *et al.* 2015, Mohamad, Rahim *et al.* 2016) and the ratio of pipeline thickness and diameter (Daoye, Bin *et al.* 2009, Altabey 2016), later Altabey (2016) found that the ECS environment temperature is effect on ECS sensitivity and sensitive domain of ECS electrodes with high percentage, so the environment temperature is the fourth factor of factors which have influence on ECS measurement sensitivity.

The objective of this study is to develop a new non-destructive evaluation (NDE) technique for detecting and predicting the crude oil types transfused inside glass fiber reinforced epoxy (GFRE) composite pipes, as one of the most materials are utilized as transmission lines in the oil, gas, water and chemical industries instead of the steel pipe. This is due to their attractive physical, mechanical and thermal properties, particularly high stiffness and strength to weight ratio, excellent corrosion resistance and dimensional stability, this target will be achieved by detecting the local variation of the dielectric properties of the fluid inside the pipe at normal temperature ($\theta = 25℃$) using an electrical capacitance sensor (ECS), and using the data coming from the sensory system to predict another types of fluids by designing and training an efficient artificial neural network (ANN) architecture is Radial Basis neural network (RBNN), with taking in to account the flow rate velocity and pressure effect. The simulation results are obtained using ANSYS and MATLAB software. The results show the excellent agreement between FE results and with RBNN results.

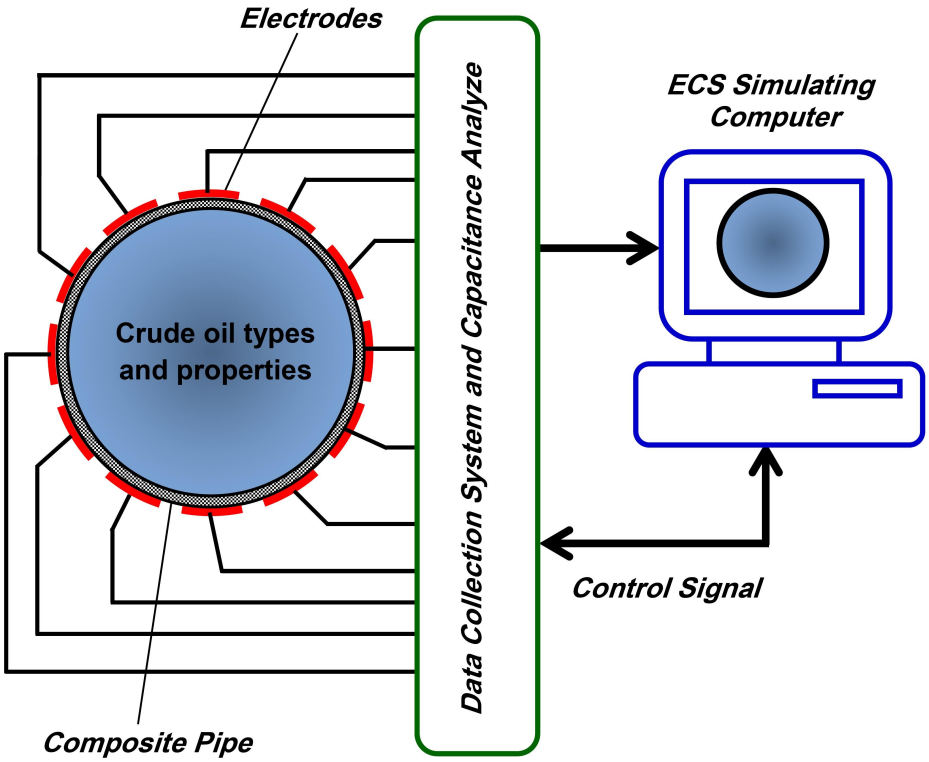

Fig. 1 Sketch of ECS system

2. Electrical Capacitance sensor (ECS)

ECS consists of insulating pipe, measurement electrode, radial screen and earthed screen (Yang and York 1999). The measurement electrodes are mounted symmetrically around the circumference of pipeline. Radial screen is fitted between the electrodes to cut the electro-line external to the sensor pipeline and reduce the inter-electrode capacitance. The earthed screen surrounds the measurement electrodes to shield external electromagnetic noise. In most application, ECS electrodes are mounted outside the pipeline which is called external electrode ECS (Yang 1997). Electrical capacitance system includes sensor, capacitance measuring circuit and imaging computer is shown in Fig. 1.

ECS converts the permittivity of inner media flow to inter-electrode capacitance, which is the ECS forward problem. Capacitance measuring circuit takes the capacitance data and transfers to imaging computer. Imaging computer reconstructs the distribution image with a suitable algorithm, which is called ECS inverse problem.

2.1 The ECS geometrical model

The model section comprises of an ECS column with 0.1 m inner diameter and 0.3 m height. The ECS is made up of GFRE composite material and having a ring of 12 electrodes (which are

separated from each other by small gap) on its outer periphery. Fig. 2 shows the cross section of 12-electrode ECS system, in which R_1 is inner pipe radius; R_2 is outer pipe radius; R_3 is earthed screen radius. The ECS also includes radial guard electrodes to constrain the field lines from the excited electrode and reduce the dependence of spacing between the electrodes and the screen as shown in the Figure. The function of the sensor includes measuring the capacitance between all possible combination pairs of the electrodes and converting the measured capacitance values in to the voltage signals. The sensors physical specification and the permittivity values of GFRE composite pipe are shown in Table 1.

Table 1 Sensor physical specification

ECS system	**Specification**
No. of electrodes	12
Space between electrodes	2 mm
Inner/outer pipe diameter	94/100 mm
Earth Screen diameter	110 mm
Thickness of electrodes	1mm
End guards	50 mm
Permittivity glass fiber/Epoxy	$\varepsilon_g = 3.12$ Fm^{-1}
Excitation voltage	$\varphi = 15$ Volts

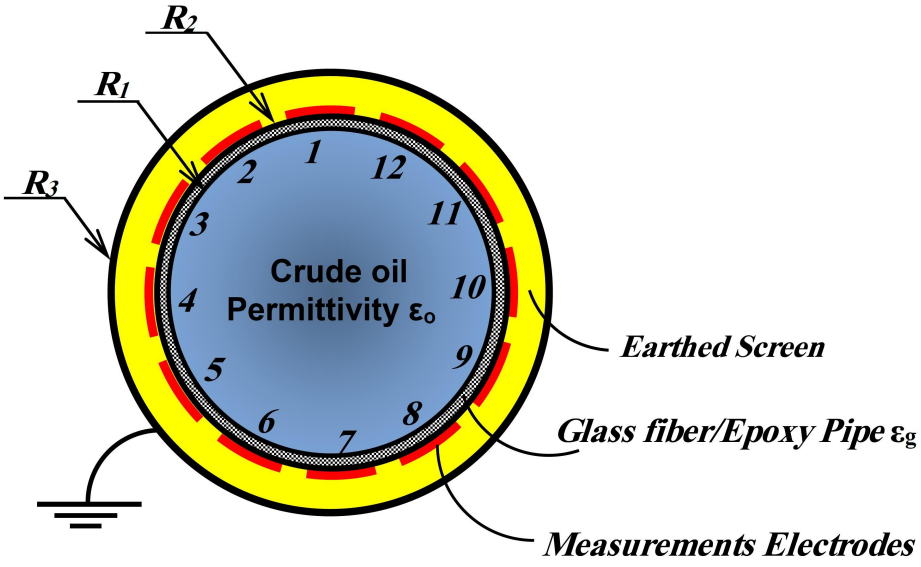

Fig. 2 Cross section sketch of 12-electrode ECS

Table 2 Permittivity coefficient ε_o for the common crude oil types

Crude oil (C.O) types according to gulf countries	**Permittivity coefficient ε_o**
Air	$\varepsilon_a = 1\ Fm^{-1}$
Saudi Arabia (oil_1)	$\varepsilon_{o_{SA}} = 2\ Fm^{-1}$
United Arab Emirates UAE (oil_2)	$\varepsilon_{o_{UAE}} = 2.2\ Fm^{-1}$
Kuwait (oil_3)	$\varepsilon_{o_{Ku}} = 3.75\ Fm^{-1}$
Qatar (oil_4)	$\varepsilon_{o_{Qa}} = 3.8\ Fm^{-1}$
Bahrain (oil_5)	$\varepsilon_{o_{Bh}} = 4.15\ Fm^{-1}$
Iraq (oil_6)	$\varepsilon_{o_{Iq}} = 4.2\ Fm^{-1}$
Oman (oil_7)	$\varepsilon_{o_{Om}} = 5.38\ Fm^{-1}$
Iran (oil_8)	$\varepsilon_{o_{Ir}} = 7.14\ Fm^{-1}$
$Water$	$\varepsilon_w = 80\ Fm^{-1}$

Data is adapted from: Saudi Aramco (2008), Saudi Aramco (2014)

2.1.1 The physical properties of crude oil inside pipeline

The measured electrical quantity of the crude oil types inside the pipe is depends on the conductivity and permittivity of the crude oil type. Permittivity is an electrical property that will be different for each of the crude oil type components, (permittivity is also sometimes called the dielectric constant). The permittivity can be measured using a capacitance sensor. The electrodes will act as a capacitance detector and the resulting capacitance can be measured between the electrodes. These capacitance will therefore vary when the permittivity changes, i.e., according to the type of crude oil. Table 2 shows the permittivity coefficient ε_o for the common crude oil types are mining in the gulf countries include Iran, Iraq, Saudi Arabia, Kuwait, Bahrain, Oman, Qatar, and the United Arab Emirates, comparing with permittivity coefficient of air and water.

2.2 The ECS composition and working principle

For 12-electrode system, the electrodes are numbered as shown in the Fig. 3, are excited with an electric potential, one at a time in increasing order, when one electrode is excited, the other electrodes are kept at ground potential as shown in the Fig. 3 and act as detector electrodes. When electrode No. 1 is excited with a potential, the change $\mathrm{Q_{1,j}}$ is induced on the electrodes, $\mathrm{j} = 2, \cdots \cdots, \mathrm{N}$ can be measured. Next, electrode No. 2 is excited whereas, rest the electrodes are kept at ground potential, and the induced charges $\mathrm{Q_{23}}, \mathrm{Q_{24}}, \cdots, \mathrm{Q_{2N}}$ $(N = 12)$ are measured. The measurement protocol continues unit electrode $N-1$ is excited. Using these charge measurements, the inter electrode capacitance $\mathrm{C_{ij}}$ can be computed using the definition of capacitance (Eq. (1)) i.e.

$$C_{ij} = \frac{Q_{ij}}{\Delta V_{ij}} \tag{1}$$

Where Q_{ij} is the charge induced on electrode j when electrode i is excited with a known potential. V_{ij} is the potential difference between electrodes i and j $(\Delta V_{ij} = V_i - V_j)$. So the number of independent capacitance measurements $M = 66$ using Eq. (2) is

$$M = \frac{N(N-1)}{2} \tag{2}$$

It is important to note that these capacitances are dependent on the geometry of electrodes and the determined once size and location of the electrodes and the permittivity distribution $\varepsilon_o(x, y)$ are known. A change in the permittivity distribution $\varepsilon_o(x, y)$ is naturally reflected in the capacitance measurements. The actual capacitance changes measured will be very small, in the order of Pico or Femto Farad(10^{-12}F or 10^{-15}F). Sequential electrodes are referred to as adjacent electrodes; have the largest standing capacitance, while diagonally or opposing electrodes will have the smallest capacitances.

3. Finite element semulation model

In terms of Electrical Capacitance sensor (ECS), the forward problem is the problem of calculating the capacitance matrix C from a given set of sensor design parameters and a given cross-sectional permittivity distribution ε_o.

The forward model proposed for ECS (Xie, Huang *et al*. 1992) is based on finite element simulations. It is assumed that both the flow distribution and the electrical field during the measurement set are 2D and static. Changes in axial direction are neglected within the axial electrode length. Furthermore free charges in the flow are also neglected. Thus, the system obeys the following Poisson equation

$$\nabla . \varepsilon_o(x, y) \nabla \varphi(x, y) = 0 \tag{3}$$

The 2D models considered in this study were constructed using commercially available finite element software, ANSYS (The Electrostatic Module in the Electromagnetic subsection of ANSYS (2014), Al-Tabey 2012). The problem space was divided into triangular elements. In a region of ideal dielectrics and space charges, the potential distribution $\varphi(x, y)$ inside the ECS is determined by solving the Poisson's equation. For the boundary condition imposed on the ECS head by the measurement system, the potential distribution $\varphi(x, y)$ can be found. The electric field vector $E(x, y)$, the electric flux density $D(x, y)$ and the potential function $\varphi(x, y)$ is related as follows

$$E(x, y) = -\nabla \varphi(x, y) \tag{4}$$

$$D = \varepsilon_o(x, y) E(x, y) \tag{5}$$

The change on the electrodes, and hence the inter electrode capacitances can be found using the definition of the capacitance and Gauss's law based on the following surface integral

$$Q_{ij} = \oint_{S_j} (\varepsilon_o(x, y) \nabla \varphi(x, y) . \hat{n})\, ds \tag{6}$$

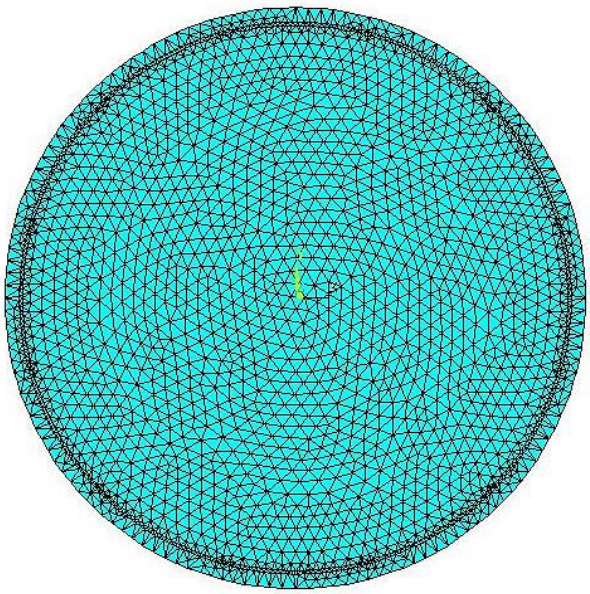

Fig. 4 (9798) Element map of finite element mesh

Where: $\varepsilon_o(x,y)$ is permittivity distribution, $\nabla.$ is divergence operator, ∇ is gradient operator, S_j is a surface enclosing electrode j, ds is an infinitesimal area on electrode j, $\hat{n}$ is the unit vector normal to S_j and ds is an infinitesimal area on it.

3.1 The boundary conditions

The potential boundary conditions were applied to the sensor-plate (electrodes). For one electrode, the boundary condition of electric potential ($V=V_0$) with 15V (V_0) was applied and another electrode was kept at ground (V=0) potential to simulate a 15V (RMS) potential gradient across the electrodes. For representing the natural propagation of electric field, the default boundary condition of continuity $(\hat{n}.(D_1 - D_2) = 0)$ was maintained for the internal boundaries.

3.2 The field partition

According to finite element analysis, we will carry out imaging of regional triangulation, it is necessary to divided pixel pipe into triangular finite element, because many pipes are round under the circumstances of a smaller number of pixels, we can achieve higher accuracy to use the triangle mesh than rectangular grids, To improve the accuracy of mesh, we will take subdivision method two times imaging region is divided into 4845 Elements. To improve the accuracy of mesh, we divided the meshed region again into 9798 Elements; the map is as follows in Fig. 4.

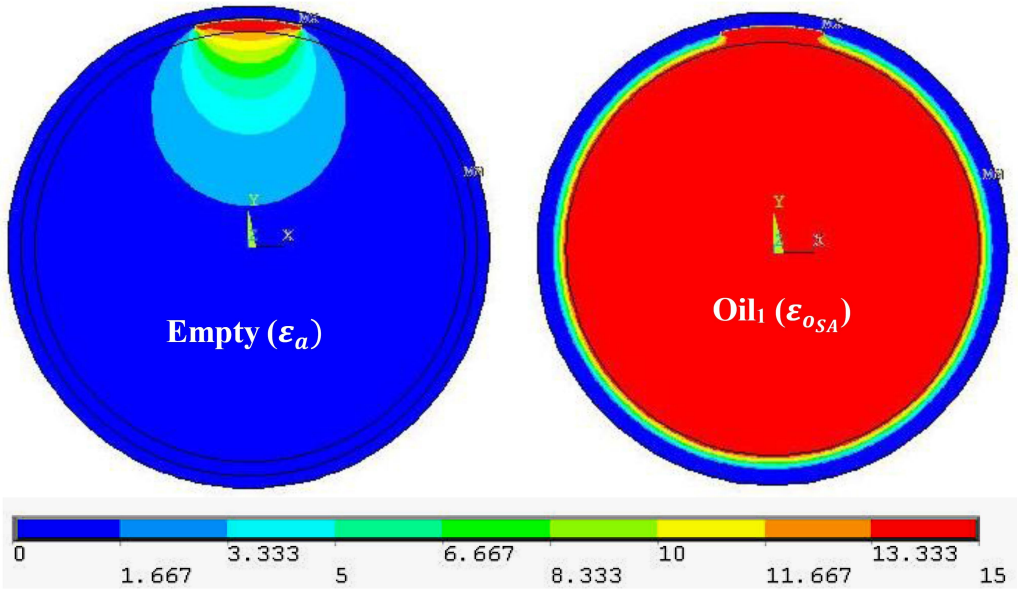

Fig. 5 The node potential distribution (Volt) of empty pipe (ε_a) right and full pipeline with oil$_1$ ($\varepsilon_{o_{SA}}$) left

4. Results and discutions

4.1 The crude oil types detection

The approach taken by ANSYS 2D is to divide the different materials and geometries into triangular elements as shown in Fig. 4, and to represent the electric field (see Eq. (4)) within each element with a separate polynomial. The software only computes the potential and the electric field values at the element nodes and interpolate between these nodes to obtain the values for other points within the elements.

The Simulations, and node potential distribution of empty (ε_a) and full pipeline with oil$_1$ ($\varepsilon_{o_{SA}}$) for the ANSYS 2D simulation, when electrode 1 is excited at normal temperature ($\theta = 25℃$), are illustrated in Fig. 5 right and left respectively.

The blue area represents the region of the pipe without potential i.e., $\varphi = 0$ but the colored areas represent the region of the pipe have the different potential (different node potential) i.e. the domain of electrode can be sensitive or detection domain. The red area represents the effect of the oil inside pipe on the node potential distribution when the pipe filling with was oil, and one electrode is excited; this means that high sensitivity to detect the change of fluid permittivity inside pipes.

Using the scripting capabilities in ANSYS we can be simulated the M=66 capacitance measurements, for crude oil types. The 66 capacitance measurements from 2D ANSYS model for three types of crude oil are mining from gulf countries (oil$_1$ ($\varepsilon_{o_{SA}}$), oil$_2$ ($\varepsilon_{o_{UAE}}$) and oil$_6$ ($\varepsilon_{o_{Iq}}$)) comparing with Air ε_a and water ε_W at ($\theta = 25℃$) are illustrated together in Fig. 6.

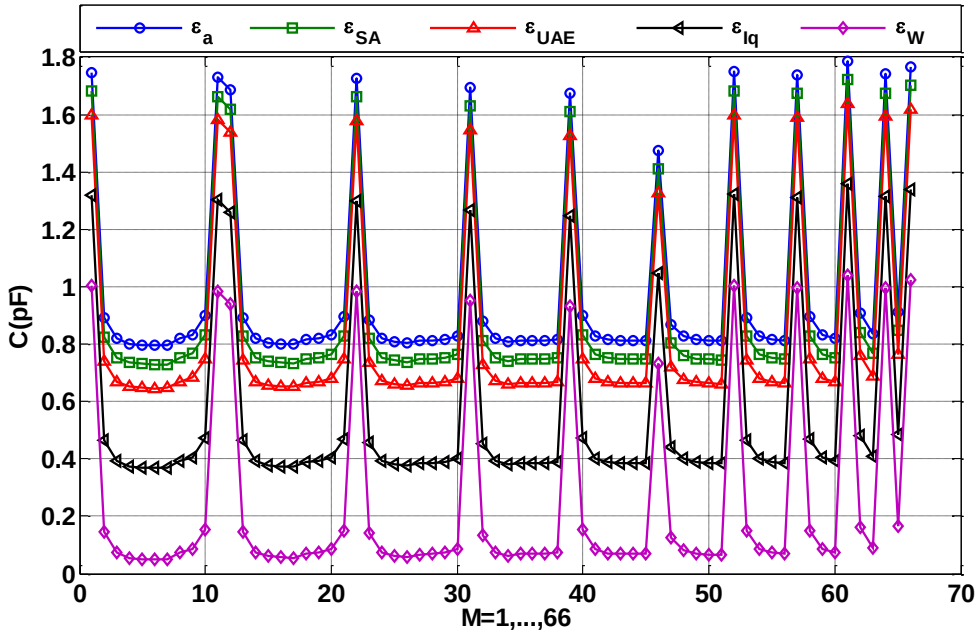

Fig. 6 Simulated capacitances from 2D ANSYS model for three types of crude oil (oil$_1$ ($\varepsilon_{o_{SA}}$), oil$_2$ ($\varepsilon_{o_{UAE}}$) and oil$_6$ ($\varepsilon_{o_{Iq}}$)) at $\theta = 25℃$

As shown in the Figs. 5 and 6 of model with permittivity changes we notice that the effect of the crude oil type changes inside GFRE pipe on the node potential distributions and capacitances values. When the primitively coefficient (ε_o) inside the pipe increase from value 1.0 for air to 80 for water through different of permittivity values for crude oils, the node potential distributions and capacitances values decrease. So the node potential distributions depended on the type of the crude oil inside GFRE pipelines.

The tendency curve of capacitance change against permittivity coefficient (ε_o) is shown in Fig. 7. In first electrode pair, capacitance change decrease monotonously with the increase of primitively coefficient. Using the power formula (7) to fit the FE results of capacitance change have proved its suitability by giving acceptable values for the correlation factor (C.F) are very near to unity. The values of three constants (Crude Oil permittivity constants) a_{ij}, b_{ij} and k_{ij} are displayed in Table 3.

$$C_{ij} = a_{ij}{\varepsilon_o}^{b_{ij}} + k_{ij} \tag{7}$$

Where $a_{ij=}\varepsilon_a$ is air permittivity coefficient, it is the permittivity baseline constant, b_{ij} is crude oil constant and k_{ij} is tendency constant between electrodes i and j, (i, j = 1,2,3,……,12).

Fig. 8 shows the sensor sensitivity versus the permittivity inside the pipeline (ε_o). The sensor sensitivity is defined as

$$Sensor\ sensitivity\% = \frac{C_a - C_o}{C_a} \times 100 \tag{8}$$

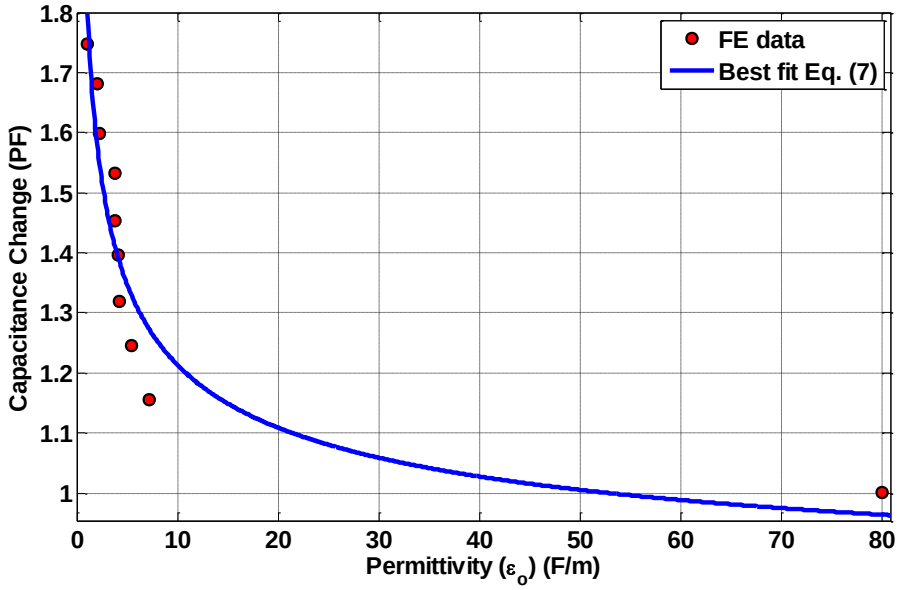

Fig. 7 Effect of crude oil type changes inside GFRE pipe on Capacitance measurements

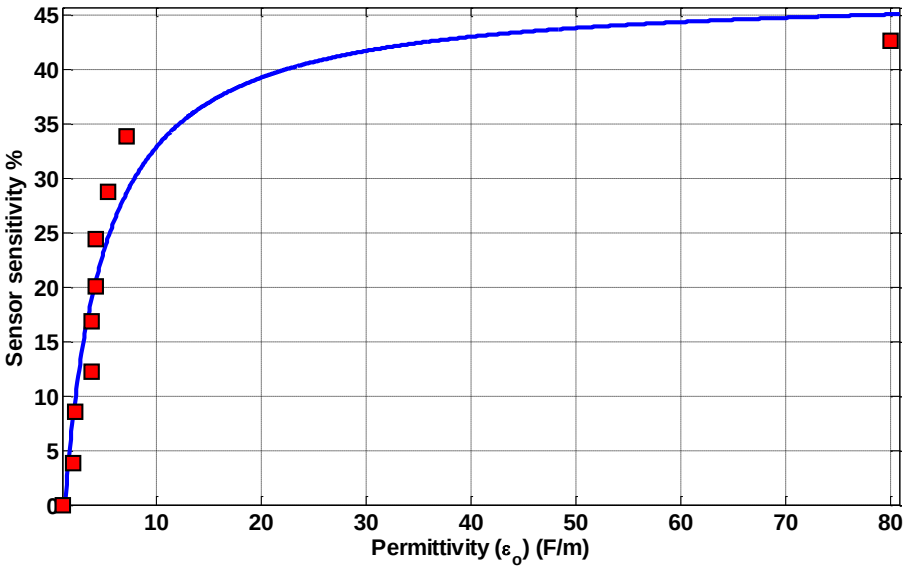

Fig. 8 Capacitance sensor sensitivity versus permittivity inside the pipeline (ε_o)

Where C_o and C_a are the capacitance measurements for permittivity inside pipeline and air permittivity respectively. The sensor sensitivity increases with the increase in the absorption time, t as the sensor has a sensitivity ranging between 3.7777and 42.6421% for permittivity ranging between 2 for oil$_1$ ($\varepsilon_{o_{SA}}$) and 80 for water (ε_W) and selected sensor geometrical parameters.

5. Artificial neural network (ANN) modeling

Artificial neural network (ANN) is an attractive inductive approach for modeling non-linear and complex systems without explicit physical representation and thus provides an alternative approach for modeling hydrologic systems. Artificial neural network was first developed in the 1940s. Generally speaking, ANNs are information processing systems. In recent decades, considerable interest has been raised over their practical applications. Training of artificial neural network enables the system to capture the complex and non-linear relationships that are not easily analyzed by using conventional methods such as linear and multiple regression methods and the network is built directly from experimental or numerical data by its self-organizing capabilities. Based on the different applications, various types of neural network with various algorithms have been employed to solve the different problems. In this work will be using the preferred ANN structures to predict the ECS capacitance change of presented numerical conditions.

5.1 Radial Basis neural networks (RBNN)

The RBNN has three layers consisting of input, a single hidden layer (function) and an output layer. The input layer is comprised of input data and the output layer yields the response of the network. The function layer is an intermediate layer between the input and the output layer. The activation function of the hidden layer neurons are a Gaussian transfer function.

$$\Phi(x) = exp\left[-\left(\sum_{j=1}^{jj}\|x_j - c_i\|^2/2\sigma_i^2\right)\right] \tag{9}$$

Where (x) is the input vector, c_i is the center of a region called a receptive field, σ_i is the width of the receptive field, $\Phi(x)$ is the output of the i^{th} neuron, and i is the number of neurons.

RBNN network can learn faster than Feed-forward neural networks (FFNN) and needs fewer number of training data. The performance of RBNN critically depends upon the chosen center where the function value is higher and the spread, that is indicative of the radial distance from the radial basis function (RBF) center, within which the function value resides, is significantly different from zero (Buhmann 2003). The spread value in this work is selected arbitrarily based on the minimum error criteria.

5.2 Performance evaluation measures

It is very useful from the designer point of view to have an neural system aids to decide whether his suggested design is suitable or not by Compute the Mean Square error MSE from equation

$$MSE = \sum\left(\left(C_{ij}\right)_{nn} - C_{ij}\right)^2/n \tag{10}$$

Where $\left(C_{ij}\right)_{\mathrm{nn}}$ is the predicted capacitance change, C_{ij} the capacitance change measured from FEM, and n is the number of FEM measured data values.

Thus, the performance index will either have one global minimum, depending on the characteristics of the input vectors. Local minimum is the minimum of a function over a limited range of input values. Local minimum is an unavoidable when the ANN is fitted. So a local minimum may be good or bad depending on how close the local minimum is to the global

minimum and how low an MSE is required. In any case, the method applied to solve this problem and descent the local minimum with momentum. Momentum allows a network to respond not only to the local gradient, but also to recent trends in the error surface. Without momentum a network may get stuck in a shallow local minimum.

5.3 Radial Basis neural networks (RBNN) Design for ECS to predict the types of the crude oil inside the pipe

A RBNN structure is designed based on two layers, the first one with radial basis neurons while the second layer with pure linear ones as shown in Fig. 9.

The training vectors formed the initial centers of the Gaussian RBFs. Determination of the hidden layer, in addition to the number of nodes in the input layer, for providing the best training results, was the initial phase of the training procedure. The target for MSE to be reached at the end of the simulations was 0.0001. Since the second step was largely a trial-and-error process, and involved RBNNs with the number of hidden layer neurons more than 10, it did not show any sizeable improvement in prediction accuracy. Thus the number of neurons (the number of RBFs) for the single hidden layer was selected as 10 neurons. Selection of the number of hidden layer neurons, with respect to the MSE term in the presence of different spread parameterized RBNNs are shown in Fig. 10.

Choosing an appropriate spread constant will increase the accuracy of the network. The spread (the width of the RBFs') constant of radial basis function was selected by using Genetic Algorithm (GA). GA may have the tendency to converge towards local optimum (Valle, Venayagamoorthy *et al*. 2008) rather than the global optimum of the problem, if the fitness function is not defined properly. The optimum spread parameter was selected as constant for all group of permittivity , after the trials with the selected hidden layer neurons number, the spread constant was selected as 0.515 (see Fig. 11).

RBNN is trained by measuring values of ε_o, θ to predict capacitance change C_{ij}. In the first RBNN structure is applied for training the data of ECS for all types of crude oil are mining from gulf countries are presented in Table 2, comparing with Air ε_a and water ε_W. Fig. 12 shows the training performance of suggested RBNN. Fig.13 represents the comparison between the FE data and the Radial Basis neural networks (RBNN) predicted data (ECS capacitance change) at $(\theta = 25℃)$ for first electrode pairs. The results of the RBNN show much satisfactory predication quality for this case study.

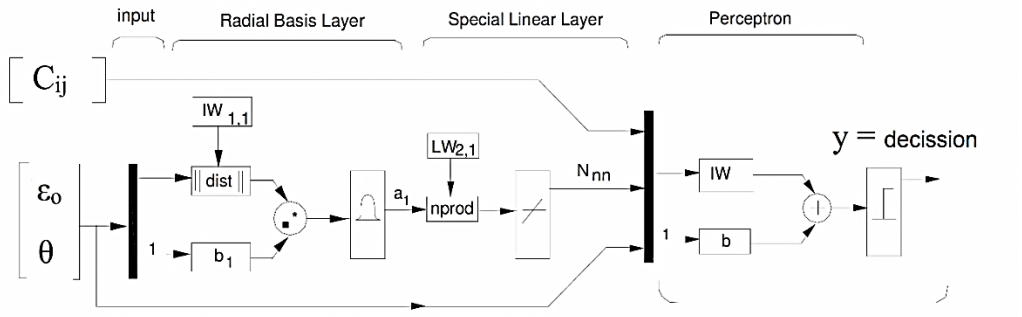

Fig. 9 Schematic illustration of RBNN design for present study with input data ε_o, θ

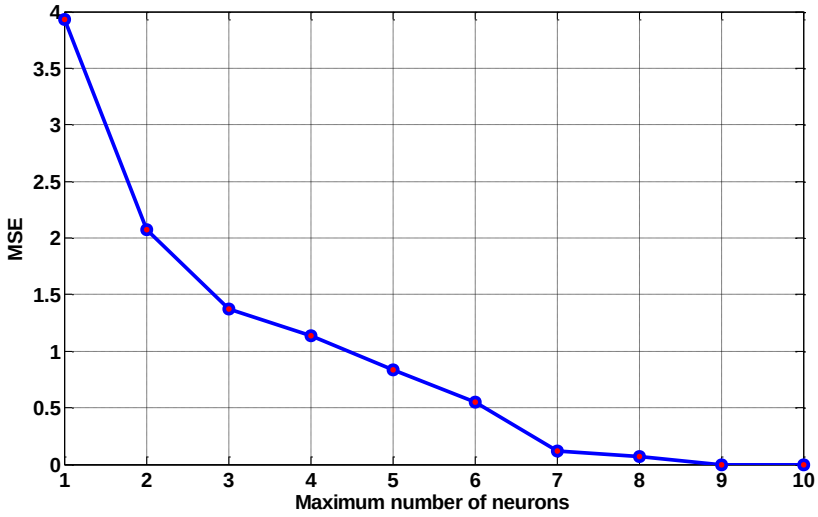

Fig. 10 Plot of MSE terms corresponding to the number of hidden layer neurons, used for selecting the optimum number of hidden layer neurons

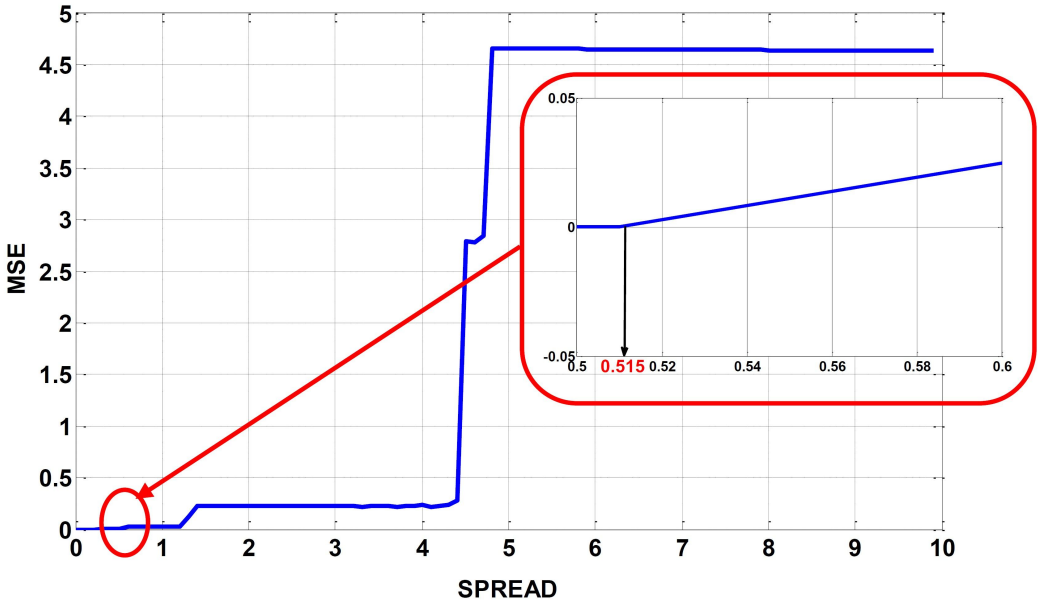

Fig. 11 Plot of MSE terms corresponding to selected spread parameters, used to select the optimum spread

The value of mean square error (MSE) between the predicted and FE data for RBNN predicted for first electrode pairs, at ($\theta = 25℃$), in order to obtain the best performances of the present network is 6.7398e-006.

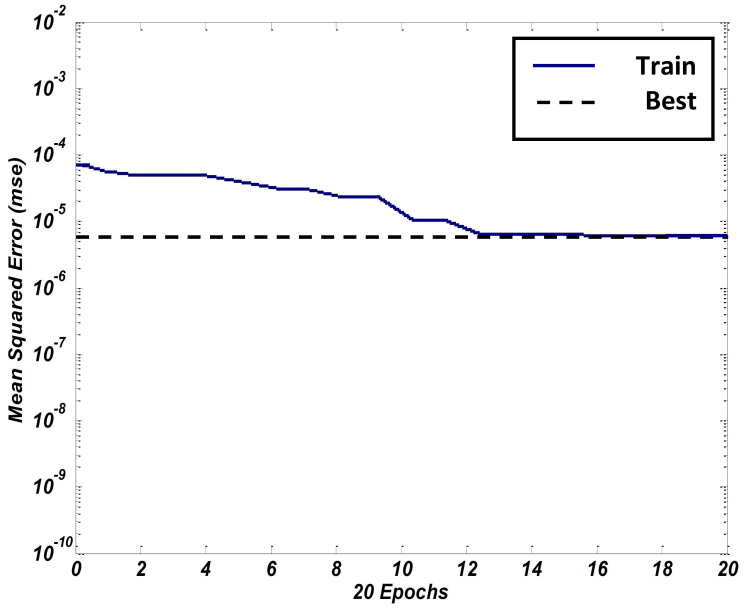

Fig. 12 Training performance of suggested RBNN

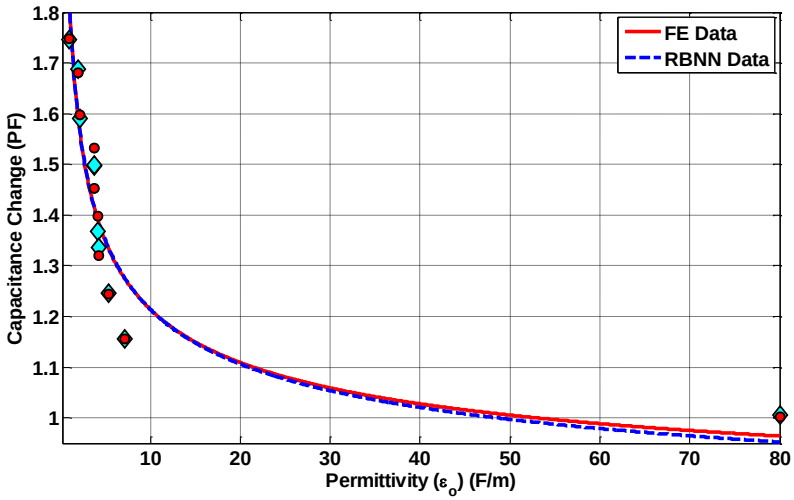

Fig. 13 Comparison between the FE data and RBNN predicted data at $\theta = 25℃$

Table 3 Crude Oil permittivity constants (a_{ij}), (b_{ij}) and (k_{ij}) at $\theta = 25℃$

	a_{ij}	b_{ij}	k_{ij}	C.F	Error in (a_{ij}) %
FE	1.083	-0.3584	0.7389	0.8801	8.3
RBNN	1.125	-0.3329	0.6912	0.8819	12.5
Avg.	1.104	----	0.71505	----	----
S.D.	0.029698	----	0.033729	----	----

6. Discussion

Fig. 13 represent the permittivity inside the pipeline (ε_o) against the capacitance change output from artificial neural network at ($\theta = 25℃$). Using the power formula $C_{ij} = a_{ij}{\varepsilon_o}^{b_{ij}} + k_{ij}$ have proved its suitability by giving acceptable values for the correlation factors (C.F) are very near to unity (see Table 3).

Comparing the result predicted from artificial neural network and data obtained from FE method for the other values of permittivity inside the pipeline (ε_o), Table 3 it is concluded that the present artificial neural network is suitable and useful in predicting FE data.

Analyzing the values of four constants (a_{ij}), (b_{ij}) and (k_{ij}) taking into account the variation of permittivity inside the pipeline (ε_o), capacitance change (C_{ij}), and considering Table 3 resulted in the following:

1) For all pipeline environment temperature (θ), at maximum points, the tendency curve of capacitance change against ε_o, for the air permittivity ε_a has the highest capacitance change and the water permittivity ε_W has the lowest capacitance change, while the crude oil permittivity for the remaining capacitance change laid in between, with descending order from $(\varepsilon_{o_{SA}})$ to $(\varepsilon_{o_{Ir}})$ with the same arrange in Table 2 respectively.
2) The deviation in the values of the constant (a_{ij}) for FE data and RBNN data may be considered constant and equal to air permittivity ε_a=1.0, the average value (Avg.) of constants (a_{ij}) was calculated of 1.104 and as the corresponding standard deviation (S.D) of 0.029698 was found to have acceptable values, as shown in Table 3.
3) The values of the constant (b_{ij}) was found to depend on the permittivity inside the pipeline (ε_o) (i.e., crude oil permittivity) and capacitance change (C_{ij}).
4) The values of the constants (k_{ij}) for FE data and RBNN data may be considered constant and equal to slope of the tendency curve the average value (Avg.) of constants (a_{ij}) was calculated of 1.104 and as the corresponding standard deviation (S.D) of 0.029698 was found to have acceptable values, as shown in Table 3.

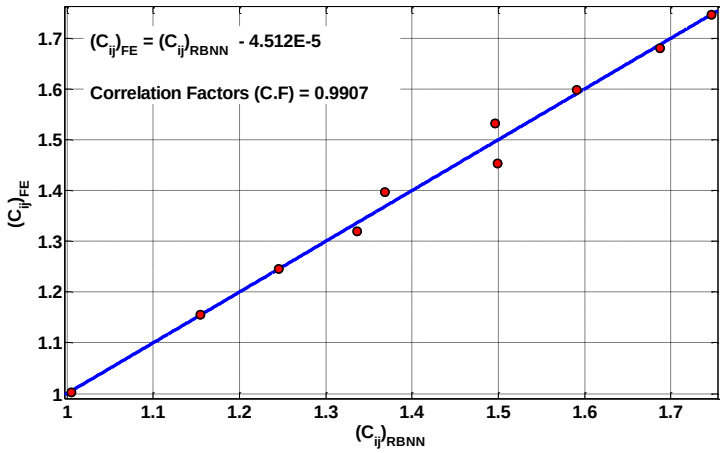

Fig. 14 FE and RBNN results correlation using ECS

7. Conclusions

For this work, the finite element method (FEM) and artificial neural network (ANN) techniques were used for modeling and simulating the electrical capacitance sensor (ECS) sensor to detect and predict the crude oil types transmitting inside GFRE pipelines, the following conclusions can be drawn:

1) The pipeline internal permittivity, i.e., decrease of the pipeline inside permittivity, was discussed completely by using FEM numerical simulation software ANSYS. Maximum capacitance change is gotten at air permittivity $\varepsilon_a = 1\, Fm^{-1}$, and the minimum the lowest capacitance change at water permittivity $\varepsilon_W = 80\, Fm^{-1}$, while the crude oils permittivity for the remaining capacitance change laid in between, with descending order from ($\varepsilon_{o_{SA}}$) to ($\varepsilon_{o_{Ir}}$) as shown in Table 2.
2) A Radial Basis neural networks (RBNN) can be used as a method for simulating the ECS to predict the FE Data of capacitance change inside the pipeline due to change in the dielectric properties inside it (i.e., the crude oil types transmitting inside pipeline) at ($\theta = 25℃$).
3) Using the power formula $C_{ij} = a_{ij}{\varepsilon_o}^{b_{ij}} + k_{ij}$ has proved its suitability for present study, and it is found that, the deviation of the constant (a_{ij}) for FE data and RBNN data with capacitance change (C_{ij}) may be considered to be constant and equal to air permittivity ε_a=1.0.
4) The value of the constant (b_{ij}) was found to be depend on the permittivity inside the pipeline (ε_o) (i.e. Crude Oil permittivity) and the capacitance change (C_{ij}) with high correlation factors (C.F).
5) The values of the constants (k_{ij}) for FE data and RBNN data may be considered constant and equal to slope of the tendency curve.
6) Finally, Fig. 14 shows a comparison between the capacitance change (C_{ij}) obtained from the FE, $(C_{ij})_{FE}$, and that of the RBNN, $(C_{ij})_{RBNN}$. There are a good agreement between the RBNN and the FE results with a correlation factor of 0.9907. Thus validating the accuracy and reliability of the proposed expert system.

References

Al-Tabey, W.A. (2010), "Effect of Pipeline Filling Material on Electrical Capacitance Tomography", *Proceedings of the International Postgraduate Conference on Engineering (IPCE 2010)*, Perlis, Malaysia, October 16-17.

Al-Tabey, W.A. (2012), Finite Element Analysis in Mechanical Design Using ANSYS: Finite Element Analysis (FEA) Hand Book For Mechanical Engineers With ANSYS Tutorials, LAP Lambert Academic Publishing, Germany, ISBN 978-3-8454-0479-0.

Altabey W.A. (2016), "FE and ANN model of ECS to simulate the pipelines suffer from internal corrosion", *Struct. Monit. Maint.*, **3**(3), 297-314, DOI: http://dx.doi.org/10.12989/smm.2016.3.3.297.

Altabey W.A., (2016), "The Thermal Effect on Electrical Capacitance Sensor for Two-Phase Flow Monitoring", *Struct. Monit. Maint.*, **3**(4), 335-347, DOI: http://dx.doi.org/10.12989/smm.2016.3.4.335.

ANSYS Low-Frequency Electromagnetic analysis Guide, The Electrostatic Module in the Electromagnetic subsection of ANSYS, (2014), ANSYS, inc. Southpointe 275 Technology Drive Canonsburg, PA 15317, Published in the USA.

Asencio, K., Bramer-Escamilla, W., Gutiérrez, G. and Sánchez, I. (2015), "Electrical capacitance sensor array to measure density profiles of a vibrated granular bed", *Powder Technol.*, **270**, 10-19.

Buhmann, M.D. (2003). "Radial basis functions: theory and implementations", Cambridge University Press, Cambridge.

Daoye, Y., Bin, Z., Chuanlong, X., Guanghua, T. and Shimin, W. (2009), "Effect of pipeline thickness on electrical capacitance tomography", *Proceedings of the 6th International Symposium on Measurement Techniques for Multiphase Flows*, Journal of Physics: Conference Series **147**, 1-13.

Fasching, G.E. and Smith, N.S. (1988), "High Resolution Capacitance Imaging System", US Dept. Energy, **37**, DOE/METC-88/4083

Fasching, G.E. and Smith, N.S. (1991) "A capacitive system for 3-dimensional imaging of fluidized-beds", *Rev. Sci. Instr*., **62**, 2243-2251

Huang, S.M., Plaskowski, A.B., Xie, C.G. and Beck, M.S, (1989), "Tomographic imaging of two-flow component flow using capacitance sensor", *J. Phys. E : Sci. Instrum*., **22**,173-177.

Jaworski, A.J. and Bolton, G.T. (2000), "The design of an electrical capacitance tomography sensor for use with media of high dielectric permittivity", *Meas. Sci. Technol*., **11**(6), 743-757.

Li, H. and Huang, Z. (2000), "Special measurement technology and application", Zhejiang University Press, Hangzhou.

Mohamad, E.J., Rahim, R.A., Leow, P.L., Fazalul, Rahiman, M.H., Marwah, O.M.F., Nor Ayob, N.M., Rahim, H.A. and Mohd Yunus, F.R. (2012), "An introduction of two differential excitation potentials technique in electrical capacitance tomography", *J. Sensors Actuators A*, **180**, 1-10

Mohamad, E.J., Rahim, R.A., Rahiman, M.H.F., Ameran, H.L.M., Muji, S.Z.M. and Marwah, O.M.F. (2016), "Measurement and analysis of water/oil multiphase flow using Electrical Capacitance Tomography sensor", *Flow Meas. Instrum.*, **47**, 62-70.

Pei, T. and Wang, W. (2009), "Simulation analysis of sensitivity for electrical capacitance tomography", *Proceedings of the 9thInternational Conference on Electronic Measurement & Instruments (ICEMI 2009)*.

Sardeshpande, M.V., Harinarayan, S. and Ranade, V.V. (2015), "Void fraction measurement using electrical capacitance tomography and high speed photography", *J. Chem. Eng. Res. Des*., **9**(4), 1-11.

Saudi Aramco (2008), "Setting new standards for 75 years: Our Legacy, Our Future", Annual Review 2008.

Saudi Aramco (2014), "Energy is opportunity", Annual Review 2014.

Valle, Y., Venayagamoorthy, G.K., Mohagheghi, S., Hernandez, J. and Harley, R.G. (2008), "Particle swarm optimization: Basic concepts", Variants and Applications in Power Systems. IEEE Transaction on Evolutionary Computation, **12**(2), 171-195.

Xie, C.G., Huang, S.M., Hoyle, B.S., Thorn, R., Lenn, C., Snowden, D. and Beck, M.S. (1992), "Electrical capacitance tomography for flow imaging: system model for development of image reconstruction algorithms and design of primary sensors", *IEEE Proceedings-G*, **139**(1), 89-98.

Yang, W.Q. (1997), "Modelling of capacitance sensor", IEEE proceedings: Measurement Science and Technology, **144**(5), 203-208.

Yang, W.Q. and York, T.A. (1999), "New AC-based capacitance tomography system", IEEE proceedings: Measurement Science and Technology, **146**(1), 47-53.

Yang, W.Q., Beck, M.S. and Byars, M. (1995b), "Electrical capacitance tomography –from design to applications", *Meas. Control*, **28**(9), 261-266

Yang, W.Q., Stott, A.L., Beck, M.S. and Xie, C.G. (1995a), "Development of capacitance tomographic imaging systems for oil pipeline measurements", *Rev. Sci. Instrum.*, **66**(8), 4326

Zhang, W., Wang, C., Yang, W. and Wang C. (2014), "Application of electrical capacitance tomography in particulate process measurement – A review", *J. Adv. Powder Technol*., **25**, 174-188.